Research Article | Vol. 29, No. 15 / 19 July 2021 / Optics Express 24144

Optics EXPRESS

Angular Airy function: a model of Fabry-Perot etalons illuminated by arbitrary beams

DYLAN M. MARQUES,[1,*] JAMES A. GUGGENHEIM,[1,2,3] AND PETER R. T. MUNRO[1]

[1] Department of Medical Physics and Biomedical Engineering, University College London, London, UK
[2] Institute of Cardiovascular Sciences, University of Birmingham, Birmingham, UK
[3] School of Computer Science, University of Birmingham, Birmingham, UK
[*] dylan.marques.17@ucl.ac.uk

Abstract: Fabry-Perot (FP) etalons are used as filters and sensors in a range of optical systems. The reflected and transmitted fields associated with an FP etalon have traditionally been predicted by the Airy function, which assumes a plane wave illumination. FP etalons are, however, often illuminated by non-collimated beams, rendering the Airy function invalid. To address this limitation, we describe the angular Airy function which calculates the reflected and transmitted fields for arbitrary illumination beams, using angular spectrum decomposition. Combined with realistic models of the experimental illumination beams and detection optics, we show that the angular Airy function can accurately predict experimental wavelength resolved intensity measurements. Based on the angular Airy function, we show that the fundamental operating principle of an FP etalon is as an angular-spectral filter. Based on this interpretation we explain the asymmetry, broadening and visibility reduction seen on wavelength resolved intensity measurements from high Q-factor FP etalons illuminated with focused Gaussian beams.

1. Introduction

A Fabry-Perot (FP) etalon is an optical cavity formed between two parallel mirrors [1]. FP etalons are typically illuminated with a collimated beam and used as optical wavelength filters [2]. They are also illuminated with non-collimated beams for applications such as non-diffracting beam generation [3], temperature sensing [4], and ultrasound sensing [5–7]. An accurate model of such applications could be used to understand the performance of such systems, the fundamental limits and even to calculate the optimal FP etalon design. For example, using a model to compute the optimal mirror reflectivities of an FP etalon for spatially resolved ultrasound sensing [8].

A few models have been applied to predict the transmitted/reflected field from FP etalons illuminated with non-collimated beams. The simplest model is the Airy function, which describes the FP etalon based on its mirror reflectivities and optical cavity thickness [9]. However, the Airy function assumes plane wave illumination and therefore is not accurate for applications using non-collimated beams. This non-validity is clear when analysing wavelength resolved intensity measurements, typically called the Interferometer Transfer Function (ITF), from a high Q-factor FP etalon illuminated with focused Gaussian beams [10]. The Airy function fails to predict the asymmetry, broadening and reduced peak transmissivity observed in those situations.

A previously reported ITF model was experimentally validated by comparing experimental and modelled ITFs measured from a high Q-factor FP etalon illuminated with a focused Gaussian beam [11]. The excellent agreement between experimental and modelled data was achieved not only through rigorous modelling of the FP etalon but also through an accurate description of the illumination beam and the impact of the detection optics. The fields reflected and transmitted by the FP etalon were calculated by treating the FP etalon as a multilayer dielectric structure. Therefore, the model requires knowledge regarding the thickness and refractive index of all layers forming the FP etalon, including the mirrors. Unfortunately, in most situations, only the mirror

#431362 https://doi.org/10.1364/OE.431362
Journal © 2021 Received 14 May 2021; revised 18 Jun 2021; accepted 23 Jun 2021; published 14 Jul 2021

Optics EXPRESS

reflectivities and optical cavity thickness of an FP etalon are known accurately, making use of this model difficult.

A different approach to simulating FP etalons illuminated with non-collimated beams is to extend the Airy function to simulate arbitrary beams [12,13] creating, what we refer to as, the angular Airy function. When compared against the dielectric multilayer model mentioned above, the angular Airy function has the advantage of describing the FP etalon based on only its mirror reflectivities and optical cavity thickness. In this work, we generalize the angular Airy function to calculate both the reflected and transmitted fields from an FP etalon. We used it to simulate an experimental FP etalon based optical system using a description of the illumination beam and detection optics representative of our experiment. This allowed us to experimentally validate the angular Airy function, for the first time, by comparing experimental and modelled ITFs. Finally, by analysing the transmitted fields predicted by the angular Airy function we explain the optical characteristics of an FP etalon and we link that explanation to features measured in the ITF.

2. Model

We begin by explaining how to calculate the fields reflected and transmitted by an FP etalon using the angular Airy function, given a particular illumination beam. In practice, the illumination beam can be calculated using models representing the illumination optics [11] or, more simply, the beam can be assumed to a have particular profile, such as a Gaussian beam [13].

The FP etalon itself is a form of multiple beam interferometer where beams undergoing varying numbers of round trips between the mirrors interfere with each other. When illuminated by a plane wave, light after each round trip can be treated as a geometric series, allowing the total reflected and transmitted light to be evaluated as an infinite sum. Equations for the reflected and transmitted fields derived in this manner are referred to as the Airy function and are given as [9]:

$$A(\theta) = \begin{cases} \sqrt{R_1} - \dfrac{(1-R_1)\sqrt{R_2}\,\exp(i\frac{4\pi}{\lambda}Nh\cos(\theta))}{1-\sqrt{R_1}\sqrt{R_2}\,\exp(i\frac{4\pi}{\lambda}Nh\cos(\theta))}, \text{ in reflection} \\ \dfrac{\sqrt{1-R_1}\sqrt{1-R_2}\exp(i\frac{2\pi}{\lambda}Nh\cos(\theta))}{1-\sqrt{R_1}\sqrt{R_2}\exp(i\frac{4\pi}{\lambda}Nh\cos(\theta))}, \text{ in transmission} \end{cases}, \tag{1}$$

where R_1 and R_2 are the reflectivities of the first and second mirrors respectively, N is the complex refractive index of the cavity, h the cavity thickness, θ the polar plane wave direction of propagation and λ is the light wavelength in vacuum. The ITF for plane wave illumination is predicted by the square modulus of $A(\theta)$ in Eq. (1).

A beam is generally thought as a field distribution in space. By applying a Fourier transform to the field complex amplitude spatial distribution in a plane, a field can be represented as a distribution of plane waves propagating with different directions and complex amplitudes, i.e., as an angular spectrum of plane waves [14]. As an example, for an Gaussian beam in the focal plane, the angular spectrum is given as:

$$\hat{E}_i(\theta,\phi) = \mathcal{F}\left(\exp\left(-4\frac{x^2+y^2}{(2\omega_0)^2}\right)\right) = \frac{(2\omega_0)^2\pi}{16}\exp\left(-\frac{k^2(2\omega_0)^2\sin(\theta)^2}{16}\right), \tag{2}$$

where $\mathcal{F}$ is the 2D Fourier transform, k is the wave number in the FP cavity ($2\pi N/\lambda$), θ and ϕ are the polar and azimuthal angles, respectively, that specify the plane wave component direction of propagation in the FP cavity and are related to the spatial frequencies (k_x, k_y) by ($k\sin(\theta)\cos(\phi)$, $k\sin(\theta)\sin(\phi)$), $2\omega_0$ is the full width at $1/e^2$ maximum of the Gaussian intensity profile, x and y are the Cartesian coordinates in the plane where the field is defined.

By assuming the illumination beam in its angular spectrum form, the Airy function can be used to computed how each illumination plane wave component is reflected/transmitted by the FP etalon. By applying this concept to all illumination plane wave components, the

Optics EXPRESS

reflected/transmitted angular spectrum can be calculated [12,13]. We refer to this approach as the angular Airy function and is defined as:

$$\hat{E}_{fp}(\theta, \phi) = \hat{E}_i(\theta, \phi)A(\theta). \tag{3}$$

The reflected/transmitted field distribution in space can be calculated with an inverse Fourier transform of the reflected/transmitted angular spectrum [14]. Having calculated the reflected/transmitted field, an additional step is required to compute the ITF. This step models the detection optics and is required to account for spatial and/or angular filtering that it might performed. Two examples used to readout FP etalons are a detector of effectively infinite extent [15] or detection with a single mode optical fibre [8], which can be modelled using Eqs. (16) and (17) of [11], respectively.

The angular Airy function is a simplified approximation of the dielectric multilayer model. In particular, (i) no phase change is experienced by light due to transmission by the mirrors, (ii) the phase of light upon mirror reflection is assumed to remain constant or change by a π factor dependent on light direction of propagation, and (iii) mirrors are assumed to be non-absorbing [9]. As these assumptions mimic the optical behaviour of dielectric mirrors, the angular Airy function is valid for modelling FP etalons with dielectric mirrors. This is confirmed by the comparison between experimental and modelled ITFs visible in Fig. 1.

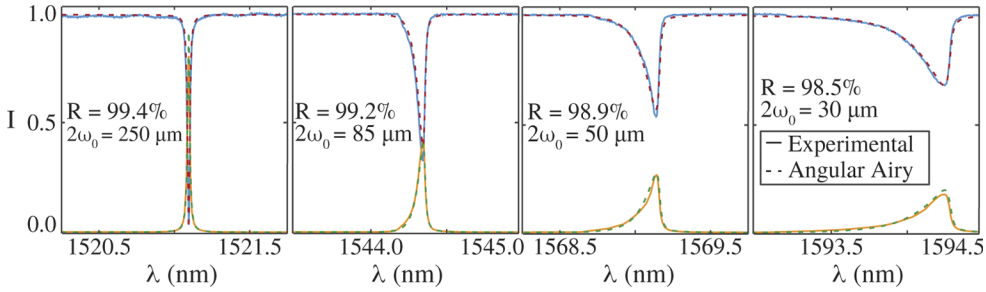

Fig. 1. Angular Airy function validation. $2\omega_0$ is the full width at $1/e^2$ maximum of the illumination Gaussian intensity profile and R the mirror reflectivities. Experimental data taken from [11]. ITFs were measured from a 102 µm thick fused silica FP etalon. The reflected and transmitted ITFs assume a single mode fibre and a detector with effectively infinite extend, respectively. The experimental ITFs were shifted along the wavelength axis to overlap the modelled data for visual comparison.

The angular Airy function does, however, have some limitations. It cannot simulate absorbing mirrors and mirrors that induce light phase changes, such as metallic mirrors. Also, the angular Airy function neglects the vectorial nature of light which is not appropriate for some applications such as for numerical apertures exceeding ~0.5 [16]. For both cases, a dielectric multilayer model is valid [11].

3. Angular-spectral filter

The angular spectrum representation of optical beams in combination with the angular Airy function provides a way of interpreting FP etalons that intuitively reveals the origins of features such as ITF asymmetry, broadening and reduced visibility which arise when focused beams are used. This interpretation is important because FP etalons have traditionally been interpreted as spectral filters. However, plane wave direction of propagation and wavelength are ambiguous for FP etalons and thus should be interpreted as angular-spectral filters [13].

To understand this, recall that for plane wave illumination, a high Q-factor FP etalon is reflective throughout most of its spectral range and becomes transparent if the plane wave is in resonance

Optics EXPRESS

inside the FP cavity. The filtering/resonance condition is achieved when the cavity optical path length matches an integer number of wavelengths and is expressed as:

$$2nh\cos(\theta) = \mathbb{Z}\lambda, \tag{4}$$

where n is the real part of the cavity refractive index and $\mathbb{Z}$ an arbitrary integer. Equation (4) shows that the FP etalon is only resonant/transparent for particular combinations of wavelength and plane wave propagation direction, hence the term angular-spectral filter. Therefore, at any wavelength, only a portion of a beam's angular spectrum satisfies the filtering condition as visible in Fig. 2(a). Since FP etalon optical performance is independent of the azimuthal angle of plane wave propagation, the transmitted angular spectrum of a rotationally symmetric illumination beam has a ring structure as visible in Fig. 2(b).

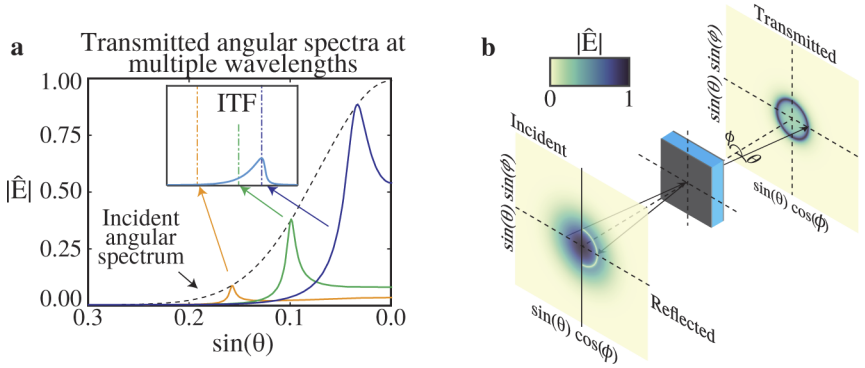

Fig. 2. (a) Computed transmitted angular spectrum assuming focused beam illumination at various wavelengths sampled by the ITF. The angular spectrum direction of propagation axis is flipped for visualization purposes. (b) Schematic showing the 2D representation of the incident, reflected and transmitted angular spectra at 1596 nm. The simulations assumes an air space etalon with cavity thickness of 10 µm and mirror reflectivities of 97 % illuminated with a Gaussian beam with spot size of 10 µm.

The first consequence of the angular-spectral nature of FP etalon is the ITF visibility being less than unity, where unity means the beam is fully transmitted. The second consequence is the broadening of the ITF, because the spectrum of plane wave propagation angles results in a spectrum of wavelengths at which resonance occurs. The third consequence is the ITF asymmetry which occurs because, as the wavelength is reduced from the normal incidence resonant wavelength, plane wave components with higher polar angles of propagation enter the filtering condition. However, as the wavelength is increased from the normal incidence resonant wavelength, there are no plane wave components in the beam's angular spectrum which enter the resonance condition.

Due to the wavelength and direction of propagation ambiguity, each wavelength sampled in an ITF has associated with it a direction of plane wave propagation which is in resonance, as illustrated in Fig. 3. Therefore, the transmitted intensity measured at each wavelength is related also to the intensity of the illumination plane wave component propagating with the associated resonant polar direction. Therefore, the ITF can be seen as a polar angular spectrum profiler.

A consequence of the ITF being an angular spectrum profiler is that the ITF broadens and has its visibility reduced as the illumination spot size reduces. This is because as spot size reduces, the width of the angular spectrum distribution increases, thus reducing the proportion of the beam's angular spectrum in resonance at any one wavelength. Furthermore, the broadening of the spectrum of propagation directions of a Gaussian beam as focal spot size decreases leads to a broader spectrum of resonant wavelengths, thus broadening the ITF.

Optics EXPRESS

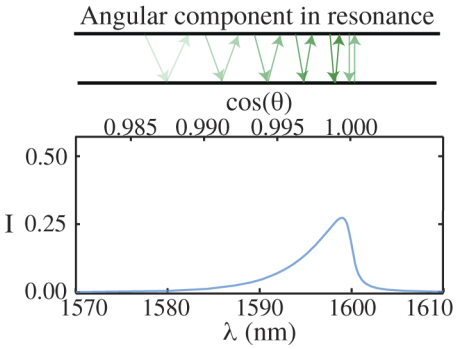

Fig. 3. ITF plotted as a function of wavelength and plane wave direction in resonance. The plane wave directions showed are just for illustrative purposes.

Understanding the impact of the FP design variables (mirror reflectivities and optical cavity thickness) on the optical response of FP etalons is critical for optimizing their design. Increasing the mirror reflectivities or the optical cavity thickness leads to a narrower angular-spectral filtering condition, as visible in the transmitted angular spectra of Fig. 4(a). This also means that a smaller proportion of the beam is in resonance, at any given wavelength, leading to a lower visibility ITF as in Fig. 4(b). This is particularly important for the design of FP etalon-based sensors. To maximize the sensitivity, the angular-spectral filtering condition must be as narrow as possible to maximise sensitivity to any induced change in the optical cavity path length. However, for maximum sensitivity, the portion of the beam that is in resonance at a given wavelength must also be maximized. With Gaussian beam illumination, these two criteria are unable to be achieved simultaneously and therefore the FP design must compromise between both.

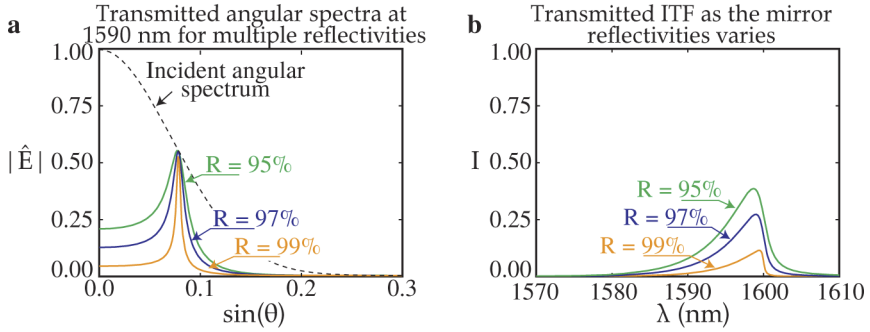

Fig. 4. Changes in the ITF and transmitted angular spectrum as the mirror reflectivity varies. Gaussian beam illumination with beam waist $2\omega_0$ of 10 µm incident upon an air space FP etalon with cavity thickness of 10 µm is assumed.

Following the previous rationale, sensitivity is maximized when the angular spectrum of the illumination beam propagates with a single polar direction. For this reason, Bessel beams, which have both narrow spatial and polar angular distributions [17], can be used for localized measurement while achieving ITF sensitivity equivalent to collimated beam illumination [18].

4. Conclusion

The angular Airy function was discussed as a model to calculate the fields reflected and transmitted by an FP etalon, requiring knowledge of only the mirror reflectivities and optical cavity thickness.

Optics EXPRESS

Coupled with models of detection optics the angular Airy function can be used to predict ITFs. We have shown that ITFs predicted with the angular Airy function accurately match experimental data, thus validating the angular Airy function. We have also used the angular Airy function to show that high Q-factor FP etalons should be considered as angular-spectral filters instead of purely spectral filters as they have typically been considered. This interpretation explains the origin of the ITF asymmetry, broadening and visibility reduction previously reported [10].

The angular Airy function is computationally inexpensive and accurate, which makes it ideal for optimizing the design of FP etalons. The angular Airy function was implemented and integrated into Jolab [19], an optical modeling environment thus allowing simulation of complex FP etalon based systems by combining models of the different components forming the system. For example, FP etalons illuminated with an axicon generated Bessel beam [18,20] or imaging FP etalon based sensors through multimode fibres [21]. The code used to compute the results shown in this paper is freely available [22].

Funding. European Research Council (741149); EPSRC Centre for Doctoral Training in Medical Imaging (EP/L016478/1); Royal Society (URF\R\191036, URF\R1\180435).

Disclosures. The authors do not declare any financial interests or conflicts of interest.

Data availability. The simulated data and code are open-source and freely available in [22].

References

1. A. Perot and C. Fabry, "On the application of interference phenomena to the solution of various problems of spectroscopy and metrology," Astrophys. J. **9**, 87 (1899).
2. T. Steinmetz, T. Wilken, C. Araujo-Hauck, R. Holzwarth, T. W. Hänsch, and T. Udem, "Fabry-Pérot filter cavities for wide-spaced frequency combs with large spectral bandwidth," Appl. Phys. B: Lasers Opt. **96**(2-3), 251–256 (2009).
3. Z. L. Horvath, M. Erdelyi, G. Szabo, Z. Bor, F. K. Tittel, and J. R. Cavallaro, "Generation of nearly nondiffracting Bessel beams with a Fabry-Perot interferometer," J. Opt. Soc. Am. A **14**(11), 3009–3013 (1997).
4. P. Morris, A. Hurrell, A. Shaw, E. Zhang, and P. Beard, "A Fabry-Perot fiber-optic ultrasonic hydrophone for the simultaneous measurement of temperature and acoustic pressure," J. Acoust. Soc. Am. **125**(6), 3611–3622 (2009).
5. E. Martin, E. Z. Zhang, J. A. Guggenheim, P. C. Beard, and B. E. Treeby, "Rapid Spatial Mapping of Focused Ultrasound Fields Using a Planar Fabry-Pérot Sensor," IEEE Trans. Ultrason. Ferroelectr. Freq. Control. **64**(11), 1711–1722 (2017).
6. A. P. Jathoul, J. Laufer, O. Ogunlade, B. Treeby, B. Cox, E. Zhang, P. Johnson, A. R. Pizzey, B. Philip, T. Marafioti, M. F. Lythgoe, R. B. Pedley, M. A. Pule, and P. Beard, "Deep in vivo photoacoustic imaging of mammalian tissues using a tyrosinase-based genetic reporter," Nat. Photonics **9**(4), 239–246 (2015).
7. K. Pham, S. Noimark, N. Huynh, E. Zhang, F. Kuklis, J. Jaros, A. Desjardins, B. Cox, and P. Beard, "Broadband all-optical plane-wave ultrasound imaging system based on a Fabry-Perot scanner," IEEE Trans. Ultrason. Ferroelectr. Freq. Control. **68**(4), 1007–1016 (2021).
8. E. Zhang, J. Laufer, and P. Beard, "Backward-mode multiwavelength photoacoustic scanner using a planar Fabry-Perot polymer film ultrasound sensor for high-resolution three-dimensional imaging of biological tissues," Appl. Opt. **47**(4), 561 (2008).
9. M. Vaughan, *The Fabry-Perot interferometer: history, theory, practice and applications* (Routledge, 2017).
10. P. La Penna, A. Di Virgilio, M. Fiorentino, A. Porzio, and S. Solimeno, "Transmittivity profile of high finesse plane parallel Fabry-Perot cavities illuminated by Gaussian beams," Opt. Commun. **162**(4-6), 267–279 (1999).
11. D. M. Marques, J. A. Guggenheim, R. Ansari, E. Z. Zhang, P. C. Beard, and P. R. T. Munro, "Modelling Fabry-Pérot etalons illuminated by focussed beams," Opt. Express **28**(5), 7691 (2020).
12. E. Nichelatti and G. Salvetti, "Spatial and spectral response of a Fabry-Perot interferometer illuminated by a Gaussian beam," Appl. Opt. **34**(22), 4703 (1995).
13. J. Y. Lee, J. W. Hahn, and H.-W. Lee, "Spatiospectral transmission of a plane-mirror Fabry-Perot interferometer with nonuniform finite-size diffraction beam illuminations," J. Opt. Soc. Am. A **19**(5), 973 (2002).
14. L. Novotny and B. Hecht, *Principles of nano-optics* (Cambridge university press, 2012).
15. E. Zhang and P. Beard, "Broadband ultrasound field mapping system using a wavelength tuned, optically scanned focused laser beam to address a Fabry Perot polymer film sensor," IEEE Trans. Ultrason. Ferroelectr. Freq. Control. **53**(7), 1330–1338 (2006).
16. P. Török, P. D. Higdon, and T. Wilson, "Theory for confocal and conventional microscopes imaging small dielectric scatterers," J. Mod. Opt. **45**(8), 1681–1698 (1998).
17. D. McGloin and K. Dholakia, "Bessel beams: Diffraction in a new light," Contemp. Phys. **46**(1), 15–28 (2005).
18. O. J. Sheppard, J. A. Guggenheim, D. M. Marques, R. Ansari, E. Z. Zhang, P. C. Beard, and P. R. T. Munro, "Interrogation of Fabry-Pérot ultrasound sensors with Bessel beams," in *Photons Plus Ultrasound: Imaging and Sensing 2020*, A. A. Oraevsky and L. V. Wang, eds. (SPIE, 2020), p. 39.

Optics EXPRESS

19. D. Marques, J. A. Guggenheim, and P. R. T. Munro, "Jolab a free and open-source software to simulate light propagation in optical systems," in *Three-Dimensional and Multidimensional Microscopy: Image Acquisition and Processing XXVIII*, T. G. Brown, T. Wilson, and L. Waller, eds. (SPIE, 2021), p. 38.
20. C. J. Zapata-Rodríguez and A. Sánchez-Losa, "Three-dimensional field distribution in the focal region of low-Fresnel-number axicons," J. Opt. Soc. Am. A **23**(12), 3016 (2006).
21. B. Keenlyside, D. Marques, M. Cherkashin, E. Zhang, P. Munro, P. Beard, and J. Guggenheim, "Wavefront shaping through multimode fibres to enable endoscopic photoacoustic tomography," in *Adaptive Optics and Wavefront Control for Biological Systems VII*, T. G. Bifano, S. Gigan, and N. Ji, eds. (SPIE, 2021), p. 14.
22. D. M. Marques, J. A. Guggenheim, and P. R. T. Munro, "Angular Airy function scripts," figshare (2021). https://github.com/DylanMMarques/Angular-Airy-Function.